



Effect of number and properties of specific sites on alumina surfaces for Pt-Al₂O₃ catalysts

Jaekyoung Lee, Eun Jeong Jang, Ja Hun Kwak*

Department of Chemical Engineering, School of Energy and Chemical Engineering, UNIST, Ulsan, South Korea

ARTICLE INFO

Keywords:

Alumina surface
Pt
Dispersion
Number of sites
Interaction strength of sites

ABSTRACT

In this work, how the number and properties of specific sites on alumina surfaces affect the specific interaction between Pt and alumina was investigated by using X-ray diffraction, ethanol temperature programmed desorption, diffuse reflectance infrared Fourier transform spectroscopy, H₂ chemisorption, scanning transmission electron microscopy and benzene hydrogenation reaction. Here, we chose two sets of model aluminas having different number of sites with the identical properties and different properties of sites with the same number based on ethanol TPD. The H₂ chemisorption results for the model aluminas show that H/Pt are all similar for low Pt loadings, but significantly different for high Pt loadings. For 1 wt% Pt/Al₂O₃, the number of specific sites on all the aluminas was sufficient to disperse all the Pt, leading to only highly dispersed Pt clusters (~1 nm). However, at 10 wt% Pt/Al₂O₃, the number of Pt atoms is greater than that of the specific sites on the alumina surface, resulting in a bimodal distribution of large agglomerated Pt (> 10 nm) and highly dispersed Pt clusters (< 3 nm) revealed by XRD and TEM. Overall, the results clearly demonstrated that Pt shows higher dispersion with increasing number of sites and interaction strength, because the Pt atoms can interact with specific sites on alumina in greater numbers and more strongly. However, these Pt dispersion changes do not represent the gradual change in Pt cluster sizes, but the relative population change of small (< 3 nm) and large agglomerated Pt clusters (> 10 nm) under bimodal distribution. The number of large agglomerated Pt clusters decreased with increasing number of sites and interaction strength. This fundamental understanding provides an important perspective for designing Al₂O₃-based supported catalysts.

1. Introduction

Pt/Al₂O₃ is one of the most important supported heterogeneous catalysts utilized in industries such as automobile exhaust combustion and petroleum refineries [1–3]. Catalytically, Pt/Al₂O₃ is mainly involved in oxidation, dehydrogenation-hydrogenation, and reforming processes [1–4]. Owing to its versatile catalytic applications in real world, the Al₂O₃-supported Pt catalyst has been of practical and fundamental interest for decades.

The catalytic properties of Pt/Al₂O₃ are affected by various parameters—size, morphology, dispersion, sintering, oxidation state, etc.—that are closely related to the specific Pt-Al₂O₃ interaction and, ultimately, the surface properties of alumina [5–10]. Therefore, numerous studies have been carried out to understand how the structural, textural, and physicochemical properties of alumina influence the supported Pt [6,10–14]. The various crystalline phases of alumina were investigated by Park et al. and they reported that Pt dispersion was affected more by crystalline structure than the surface area of alumina

[11]. Mironenko et al. showed that hydrothermal treatment of alumina increased the number of bridging OH groups, leading to weaker interaction with H₂PtCl₆ (outer-sphere complex) and lower reduction temperature [10]. It indicates that the alumina surface hydroxyl groups affect its interaction with platinum. The properties of these surface hydroxyls are known to be closely related to the activation temperature and crystal facets, as the study reported by Digne et al. [15,16]. Various effects of crystalline facets have been studied by both experimental and computational methods. Kwak et al. reported that Pt is anchored on penta-coordinated Al³⁺ sites on (100) facets by using solid-state nuclear magnetic resonance spectroscopy, scanning transmission electron microscopy, and density functional theory calculation [14]. Subsequently, Hu et al. reported that Pt₁₃ clusters favor the formation of two-dimensional (2D) rafts on dehydrated (100) surfaces, but 3D morphologies on hydroxylated (110) surfaces as revealed by DFT calculations [6]. Furthermore, Agnes et al. showed experimental evidence for the 2D-3D morphologies of Pt clusters on (100) and (110) surfaces, and further morphological changes to hydrogen coverage by combining

* Corresponding author.

E-mail address: jhkaw@unist.ac.kr (J.H. Kwak).

experimental XANES studies and DFT simulations [12]. Despite intensive research efforts to understand the effect of alumina on Pt-Al₂O₃ interaction, there are still issues to be resolved, because the structural, textural, and physicochemical properties of alumina are closely interrelated [17–19].

In order to distinguish how each parameter of alumina contributes to the Pt-Al₂O₃ interaction, systematic approaches must involve the well defined model alumina with sensitive and quantitative characterization of alumina surface properties [19–23]. Recently, we have reported that ethanol temperature programmed desorption (TPD) can sensitively characterize the number and properties of specific sites on various kinds of alumina with different morphologies, crystalline phase, and additives [24].

In this work, we investigated how the number and properties of specific sites on an alumina surface affect its interaction with Pt. In this regard, we chose two sets of model aluminas having different number of sites with the identical properties and different properties of sites with the same number based on ethanol TPD. After loading Pt onto these model aluminas, the Pt dispersion was analyzed by H₂ chemisorption, XRD, TEM and STEM. The results clearly demonstrated that Pt shows higher dispersion with increasing number of sites and interaction strength. This fundamental understanding provides an important perspective for designing Al₂O₃-based supported catalysts.

2. Experimental

2.1. Catalyst preparation

We chose four types of model aluminas. Three aluminas were supplied from Sasol company, Puralox TH 100/150, TH 200/110, and TH 500/80, and labelled as T150, T110, and T80, respectively. We calcined T150 aluminas at 1000 °C for 3 h and labelled it T1000.

0.5–10 wt% Pt/Al₂O₃ were prepared by conventional incipient wetness impregnation with Pt(NH₃)₄(NO₃)₂ in water and dried at 120 °C overnight. Note that we used Pt(NH₃)₄(NO₃)₂ as the Pt precursor in order to remove any additional Cl effect [25,26]. All the samples were calcined at 500 °C for 2 h using 20% O₂/He (1 ml/s) then reduced at 500 °C for 1 h under 10% H₂/He flow (1 ml/s).

2.2. Catalyst characterization

The XRD patterns were obtained on a Bruker D2 phaser diffractometer using Cu K α radiation ($\lambda = 1.54 \text{ \AA}$) in the step mode between 2θ values of 5 and 80°, with a step size of 0.02°/s. The tube voltage and current were 30 kV and 10 mA, respectively. The morphologies of Al₂O₃ were confirmed by TEM (JEOL JEM-2100). The specific surface areas were determined by the Brunauer-Emmett-Teller method using BELSORP-Max instrument.

Ethanol TPD was carried out using the same experimental procedures as described in our previous report [22,24,27,28]. 50 mg of alumina was calcined at 500 °C for 1 h under 20% O₂/He flow (1.0 ml/s). After calcination, the sample was cooled to room temperature and ethanol adsorption was carried out for 30 min using a 2.0% ethanol/He gas mixture (1.0 ml/s), followed by He purging for 30 min to remove weakly-bound ethanol molecules. After stabilization of the flame ionization detector (FID) signal of an Agilent 7820 A gas chromatograph (GC), a TPD experiment was carried out in flowing He (1.0 ml/s) at the heating rate of 10 °C/min, and the reactor outlet was directly connected to the FID (i.e., no GC column separation).

Diffuse reflectance infrared Fourier transform spectroscopy (DRIFTS) experiments were carried out on a Nicolet iS50 FTIR spectrometer equipped with a mercury cadmium telluride (MCT) detector to investigate the hydroxyl groups and the relative ratio of Lewis and Brønsted acid sites on alumina surface. 14 mg of Al₂O₃ was loaded into high temperature reaction chamber (Harrick Scientific) with ZnSe windows installed in a Praying Mantis diffusion reflection accessory. All

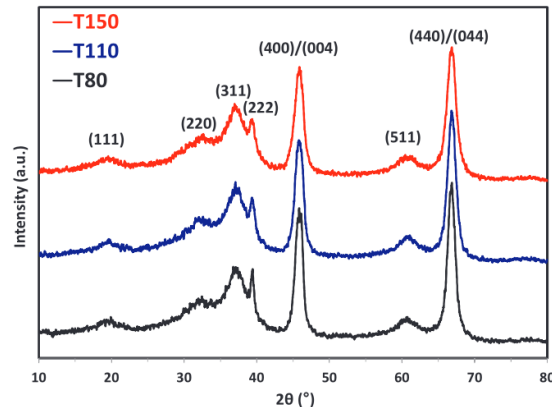


Fig. 1. XRD patterns for T150, T110, and T80.

Table 1
BET surface area of T150, T110, T80, and T1000.

Sample	BET surface area (m ² /g)
T150	143
T110	95
T80	79
T1000	100

the samples were pretreated using 20% O₂/He (flow rate = 1 ml/s) at 380 °C (this temperature was calibrated and also the maximum temperature achievable using the current DRIFTS accessory). The FT-IR spectra of the hydroxyl groups were collected at RT with KBr background. The each spectrum was normalized with the intensity of 3725 cm⁻¹ peak which was assigned to OH groups on the (110) surface by Digne et al [15]. Also, in order to observe the acid-base properties on the alumina surface, pyridine adsorption was performed with 1% pyridine/He flow at 100 °C until the sample was saturated with pyridine. The spectrum was obtained after He purging at the same temperature for 1 h to remove the weakly bound pyridine on the alumina surface by using the spectrum of the pretreated-sample itself under He flow at 100 °C as the background. All the spectra were collected with average 128 scans at the resolution of 4 cm⁻¹. The each spectrum was normalized with the intensity of 1614 cm⁻¹ peak which was assigned as pyridine on the weak acidic surface OH groups of the alumina surface [29].

Hydrogen (H₂) chemisorption was performed on Belcat-B(BEL Japan, Inc.). 50 mg of a sample was calcined at 500 °C for 2 h under 20% O₂/He (1.0 ml/s) and, subsequently, reduced at 500 °C for 1 h under 10% H₂/He (1.0 ml/s). After purging for 30 min under He (1.0 ml/s), Pt/Al₂O₃ was cooled to 40 °C and chemisorption was carried out by repeated pulse (0.319 ml loop–4% or 10% H₂/Ar). Metal dispersion was calculated based on the stoichiometry of H/Pt = 1. Average diameter of platinum was estimated by the formula of 1.1/(H/Pt) [30]. For the reduced samples, high-angle annular dark-field scanning transmission electron microscopy (HAADF-STEM) images were obtained using a JEOL 2100 F (JEOL) operated at 200 kV. The particle size distributions were obtained by measuring 400–530 clusters.

2.3. Catalyst reaction tests: benzene hydrogenation

Benzene hydrogenation was performed in a quartz flow reactor using selected Pt/Al₂O₃ samples supported by quartz wool. The samples were calcined at 500 °C for 2 h under 20% O₂/He (1.0 ml/s) and then, reduced at 500 °C for 1 h under 10% H₂/He (1.0 ml/s). After purging for 30 min under He (1.0 ml/s), Pt/Al₂O₃ were cooled to RT and ramped to 80 °C under H₂/He and stabilized before injection of C₆H₆ using a

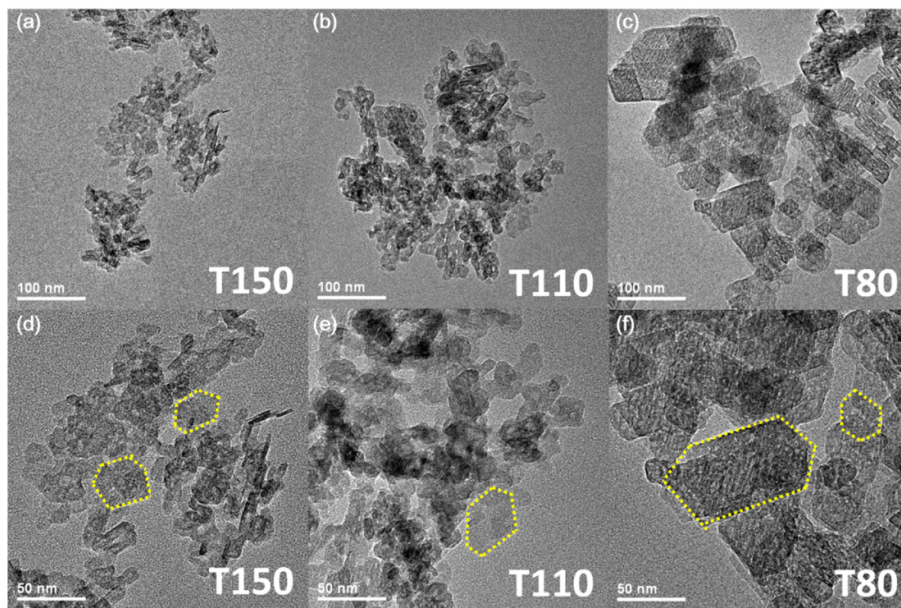


Fig. 2. TEM images for (a,d) T150, (b,e) T110, and (c,f) T80.

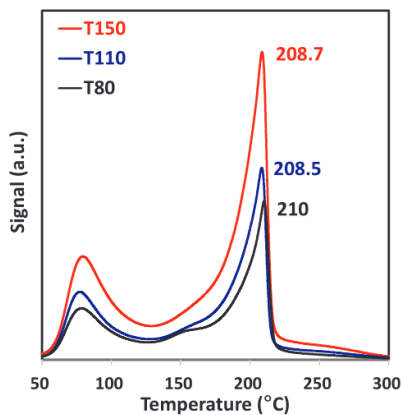


Fig. 3. EtOH TPD for T150, T110, and T80.

Table 2

Maximum desorption temperatures and amounts of dissociative ethanol from EtOH TPD for T150, T110, T80, and T1000.

Al ₂ O ₃	T _d	Dissociative EtOH (mol/g)
T150	208.7	3.8.E-04
T110	208.5	2.4.E-04
T80	210.0	2.0.E-04

syringe pump. The outlet gases were analyzed by a GC (Agilent 7820 A) with a HP-PLOT Al₂O₃ S column and FID. The reaction was carried out under 2% C₆H₆ and 10% H₂ under total flow rate of 1 ml/s with He balance. During the measurements, catalyst deactivation was observed, so the catalytic activities were compared based on the initial rates by linear extrapolation. The rate measurements were recorded in the absence of diffusion control or thermal gradients by using the Madon–Boudart criterion as described in Supporting Information (Fig. S1) [31]. The maximum benzene conversion obtained in this work was 13%.

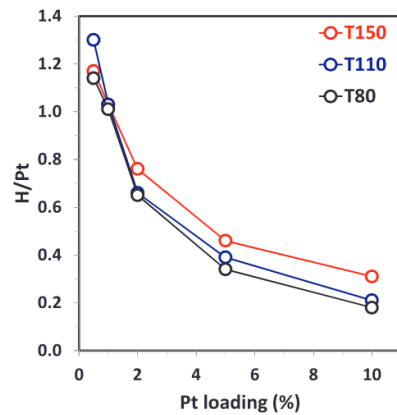


Fig. 4. H/Pt trend as a function of Pt loading for T150, T110, and T80 after calcination and reduction at 500 °C.

3. Results and discussion

In order to investigate the effect of the number and properties of specific sites on an alumina surface for Pt-Al₂O₃ interaction, we chose two sets of model aluminas having different number of sites with the identical properties and different properties but with the same number of sites. Recently, we studied the acid-base properties of alumina with various surface characteristics by ethanol TPD and reported that the desorption temperature of dissociative ethanol (at the maximum rate of ethylene desorption, T_d) can be used as a descriptor for the acid-base properties of alumina [19,24,28]. The number of sites on an Al₂O₃ surface can be determined by the amount of dissociative ethanol desorbed, and the properties of the sites by the desorption temperature (T_d) from ethanol TPD. With the aid of ethanol TPD, we chose the model aluminas T150, T110, T80 (supplied from Sasol), and T1000 (obtained by calcining T150 at 1000 °C for 3 h), and their characterizations will be detailed in the later sections.

3.1. Number of sites

The XRD diffraction pattern in Fig. 1 showed that T150, T110, and

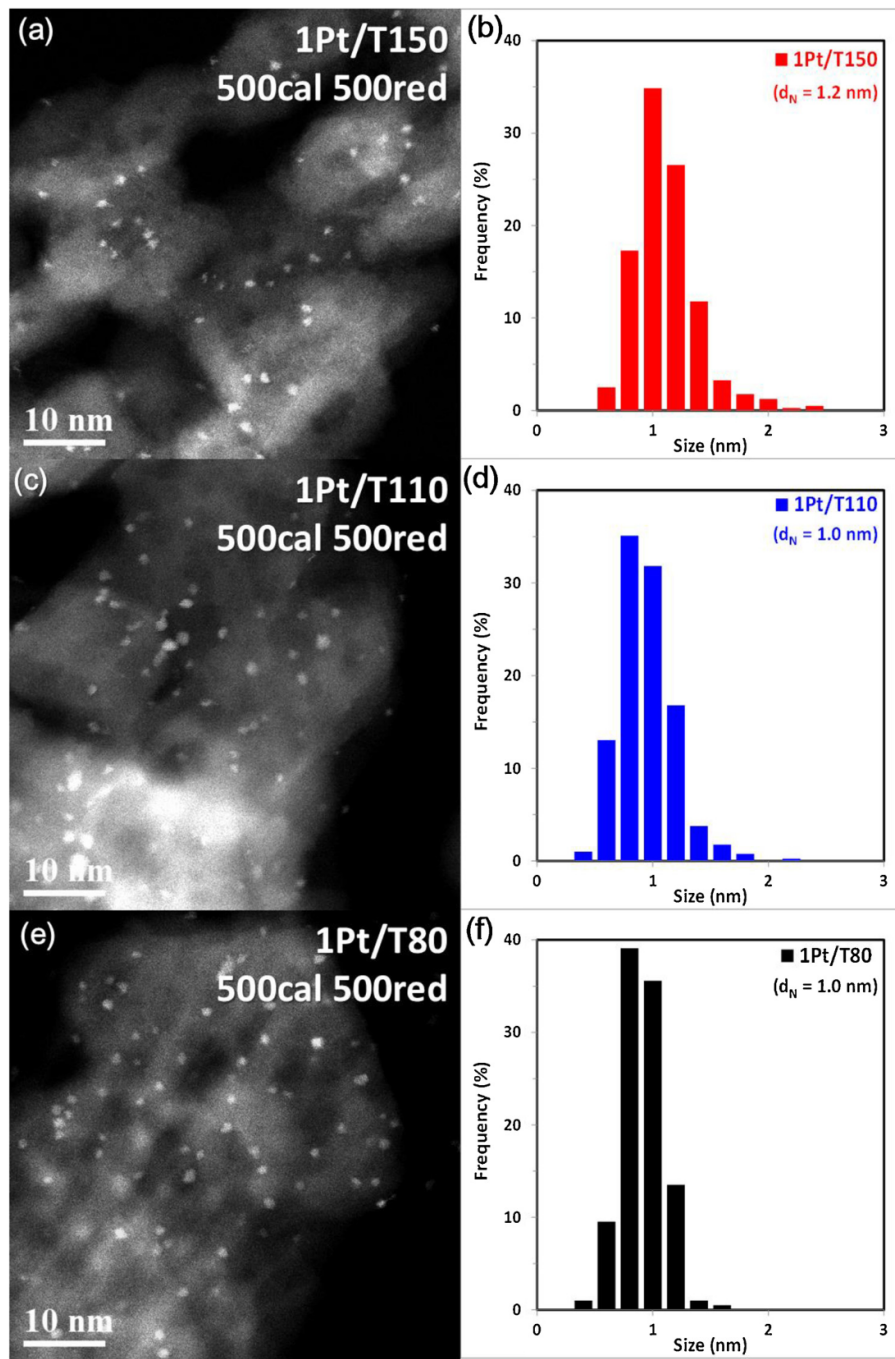


Fig. 5. STEM images and particle size distribution for (a,b) 1 Pt/T150, (c,d) 1 Pt/T110, and (e,f) 1 Pt/T80 after calcination and reduction at 500 °C.

T80 all exhibited the same bulk structure as γ-Al₂O₃ (JCPDS no. 10-425). The (222) peak at $2\theta = 39.9^\circ$ and (400)/(004) peaks at $2\theta = 45.7$ –46.7° were sharper for T80 than for T150, indicating bigger crystallites for T80 compared to T150. The BET surface areas of the three aluminas (Table 1) followed the order T150 > T110 > T80 (T150: 143 m²/g, T110: 95 m²/g, and T80: 79 m²/g). The N₂ adsorption/desorption profiles shown in Fig. S2(a) revealed very small amounts of microporosity and mesopores, and showed the H3-type hysteresis which originated from the slit-like pores of aggregated platelet particles [32]. All the aluminas had hexagonal platelet morphologies which was confirmed by TEM (Fig. 2). The only difference was in

their particle size. The particle size was the smallest for T150, the intermediate for T110, and the biggest for T80, which was consistent with the results of XRD and BET surface areas.

Ethanol TPD for T150, T110, and T80 were performed after activation at 500 °C. The TPD profiles of the three aluminas, shown in Fig. 3, were consistent with the previously reported profiles for γ-Al₂O₃ [22,24,27,33]. The desorption profiles showed two peaks, one (at < 150 °C) corresponding to weakly bound ethanol and the other (> 150 °C) to dissociatively adsorbed ethanol, which was desorbed as ethylene. Interestingly, all three aluminas showed practically the same T_d (208.5–210 °C), with the only difference being the amounts of

J. Lee et al.

Applied Catalysis A, General 569 (2019) 8–19

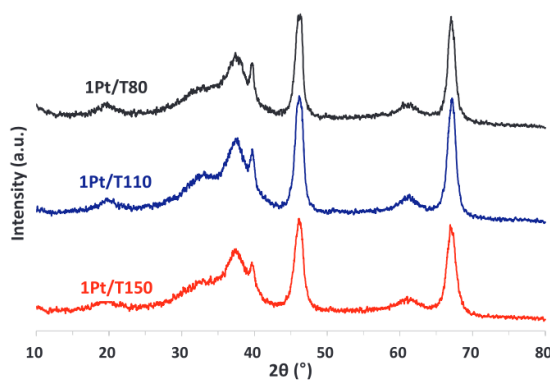


Fig. 6. XRD patterns for 1 Pt/T150, 1 Pt/T110, and 1 Pt/T80 after calcination and reduction at 500 °C.

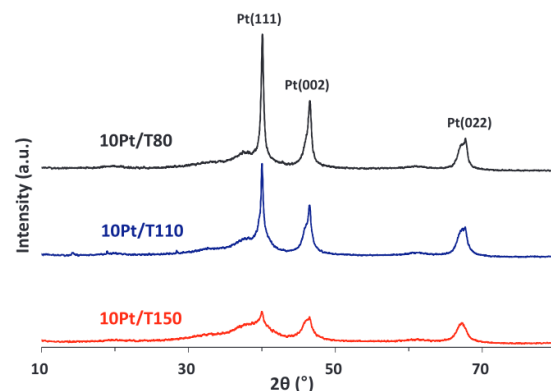


Fig. 8. XRD patterns for 10 Pt/T150, 10 Pt/T110, and 10 Pt/T80 after calcination and reduction at 500 °C.

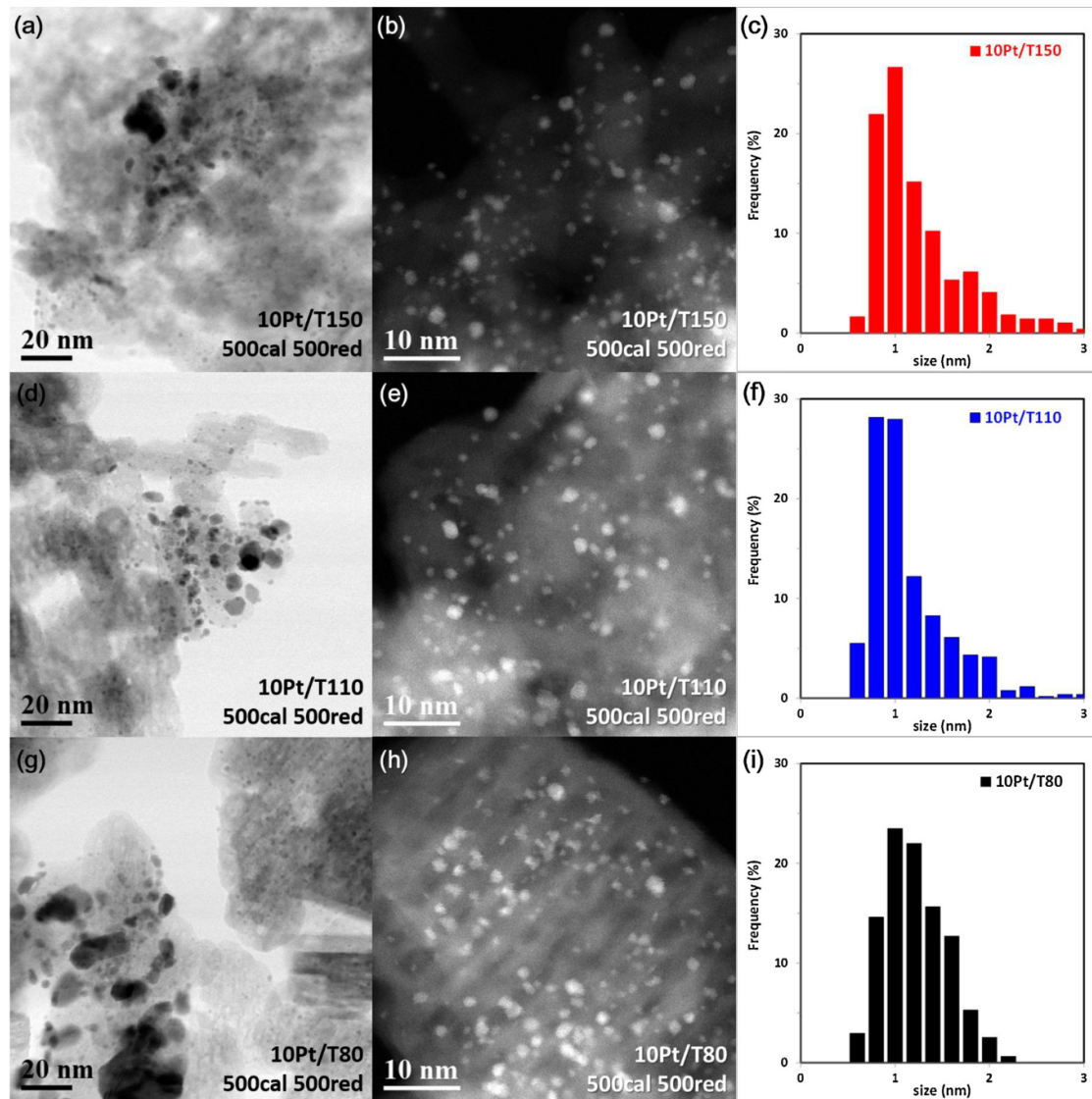


Fig. 7. Low magnification TEM, STEM images and particle size distribution below ~ 3 nm for (a–c) 10 Pt/T150, (d–f) 10 Pt/T110, and (g–i) 10 Pt/T80 after calcination and reduction at 500 °C.

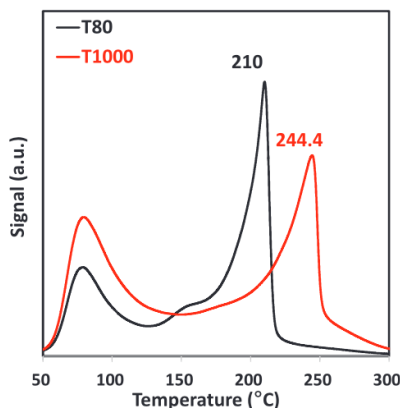


Fig. 9. EtOH TPD for T1000 and T80.

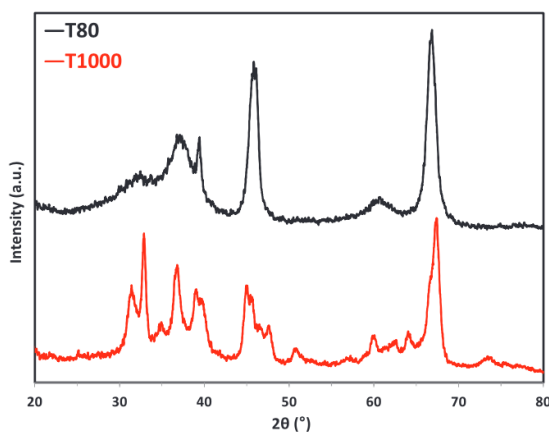


Fig. 10. XRD patterns for T1000 and T80.

dissociative ethanol desorbed (Table 2). The desorption amounts of dissociative ethanol were 3.8×10^{-4} mol/g for T150, 2.4×10^{-4} mol/g for T110, and 2.0×10^{-4} mol/g for T80, which was consistent with the trend in the BET surface area (T150 > T110 > T80).

Fig. S3(a) showed the DRIFTS spectra for surface hydroxyl groups for T150, T110, and T80 after activation at 380 °C. All spectra showed the peaks at 3766, 3725, 3670, and 3585 cm⁻¹, which was consistent with typical bands of γ-Al₂O₃ [34,35]. Even though the exact assignments of surface hydroxyls on γ-Al₂O₃ are still debated [16,17,36–40], the relative distributions of each hydroxyl band were similar, indicating the identical distribution of hydroxyl groups on the three aluminas, which exhibited the same bulk structure as γ-Al₂O₃ based on XRD and similar acidic properties, as evidenced by the same T_d obtained from ethanol TPD.

Fig. S3(b) and Fig. S3(c) showed the DRIFTS spectra after pyridine adsorption at 100 °C on T150, T110, and T80. Fig. S3(c) showed two distinctive peaks at 1623 and 1614 cm⁻¹, which were assigned to the pyridine on Lewis acid sites and the weakly acidic surface OH groups of the alumina surface, respectively [29]. The relative ratios between the 1623 and 1614 cm⁻¹ peak intensities were similar for the three aluminas. Fig. S3(b) showed the perturbed surface hydroxyls after pyridine adsorption. Furthermore, the relative ratios between the 3766 and 3722 cm⁻¹ peak for the three aluminas were similar. Overall, the IR results revealed similar acid site distributions among T150, T110, and T80 (similar properties of sites). This is consistent with the same T_d (208.5–210 °C) from ethanol TPD. In addition, the TEM image shown in Fig. 2 confirmed that all the aluminas have hexagonal morphologies, but with different particle sizes, indicating the same facet ratio.

All the results clearly demonstrate that T150, T110, and T80 can be

regarded as model aluminas having different number of specific sites with the same properties. Next, we loaded the active phase (Pt) on these model aluminas by conventional incipient wetness impregnation and studied the effects of the number of specific sites on Pt-Al₂O₃ interaction. Anchoring sites for Pt are mainly related to Lewis acid sites and also ethanol adsorbs on these sites [14,27,33,41,42]. We thought, if aluminas have different number of surface sites evidenced by ethanol TPD, then the number of Pt atoms that can interact with that defect sites on the alumina surface would be also different, leading to different Pt dispersion.

Fig. 4 showed H/Pt as a function of Pt loading from 0.5 to 10 wt%, as obtained from H₂ chemisorption after in-situ oxidation and reduction at 500 °C. Overall, H/Pt decreased with increasing Pt loading. At low loading 0.5–1 wt% Pt, H/Pt was practically the same for all the model aluminas. For 1 wt% Pt/Al₂O₃, H/Pt was 1.03 for T150, 1.03 for T110, and 1.01 for T80. However, at higher Pt loading from 2 to 10 wt%, H/Pt was the highest for T150 and the lowest for T80. At 10 wt% Pt/Al₂O₃, H/Pt was 0.31 for T150, 0.21 for T110, and 0.18 for T80, showing that Pt was better dispersed on T150 than on T80. Overall, the higher the number of specific sites on the alumina, the higher the Pt dispersion.

It is well known that Pt dispersion and morphology significantly depend on Pt loading relative to the number of anchoring sites on the alumina surface [14,43]. Quantitative high-resolution ²⁷Al-NMR studies showed that when Pt/Al₃₊^{penta} (penta-coordinated Al³⁺ sites) is one at 300 °C for calcined 1 wt% Pt/γ-Al₂O₃, Pt exists as atomically dispersed form, but 2D clusters are formed at higher Pt/Al₃₊^{penta} for higher Pt loading on γ-Al₂O₃ (2–10 wt% Pt). In addition, large aggregated Pt was detected when Pt loading increased [43]. Despite the different preparation methods used for Pt/Al₂O₃ in this study (γ-Al₂O₃ whose BET surface areas are 80–150 m²/g and 500 °C calcination and reduction), the results consistently showed that H/Pt decreased with increasing Pt loading. At 0.5–1 wt% Pt loading, the three aluminas all have sufficient number of sites to disperse all the Pt atoms. That's why the H/Pt values for T150, T110, and T80 were all 1.0, indicating highly dispersed Pt clusters on alumina surfaces. However, with increasing Pt loading to 10 wt%, the number of Pt atoms became higher than that of the anchoring sites. It leads gradual decrease of H/Pt with increasing Pt loading up to 10 wt%. The 10 wt% Pt/Al₂O₃ showed H/Pt values of 0.31–0.18, indicating that the Pt cluster size increased compared to that of 1 wt% Pt/Al₂O₃. Although all the Pt could not be highly dispersed at 10 wt% loading, T150 has twice the number of sites as T80, leading to a higher Pt dispersion on T150 (10 wt% Pt/T150: 0.31 and 10 wt% Pt/T80: 0.18), because more Pt atoms can interact with the anchoring sites on the T150 surface. In other words, T80 has less anchoring sites for stabilizing Pt, leading to more Pt sintering compared to T150.

The Pt dispersion was also confirmed by TEM measurements. Fig. 5 showed the representative STEM images for 1 wt% Pt/Al₂O₃ after calcination and reduction at 500 °C. Pt clusters around ~1 nm were highly dispersed, consistent with the absence of diffraction peak for Pt in XRD (Fig. 6) and also hydrogen chemisorption data (Fig. 4). The Pt size distribution by measuring 400 clusters on Fig. 5(b),(d) and (f) revealed that the average particle diameter was 1.2 nm for T150, 1.0 nm for T110, and 1.0 nm for T80, indicating that the Pt size was similar among the aluminas, which was consistent with the same H/Pt obtained by H₂ chemisorption. At low loading (1 wt% Pt), the number of anchoring sites is sufficient to disperse all the Pt, leading to the formation of highly dispersed small Pt clusters.

Fig. 7 showed the representative TEM and STEM images for 10 wt% Pt/Al₂O₃ after the same treatments. At high loadings, the number of Pt is much higher than that of the anchoring sites, leading to the agglomeration of Pt atoms and heterogeneous distribution on the alumina surface. The TEM images on Fig. 7(a),(d) and (g) showed both aggregated Pt (> 10 nm) and small Pt clusters (< 3 nm), indicating a bimodal distribution of Pt cluster sizes for 10 wt% Pt/Al₂O₃. Here, Fig. 7(b),(e) and (h) showed that a significant portion of Pt still existed as highly dispersed Pt with size around ~1 nm, which was similar to

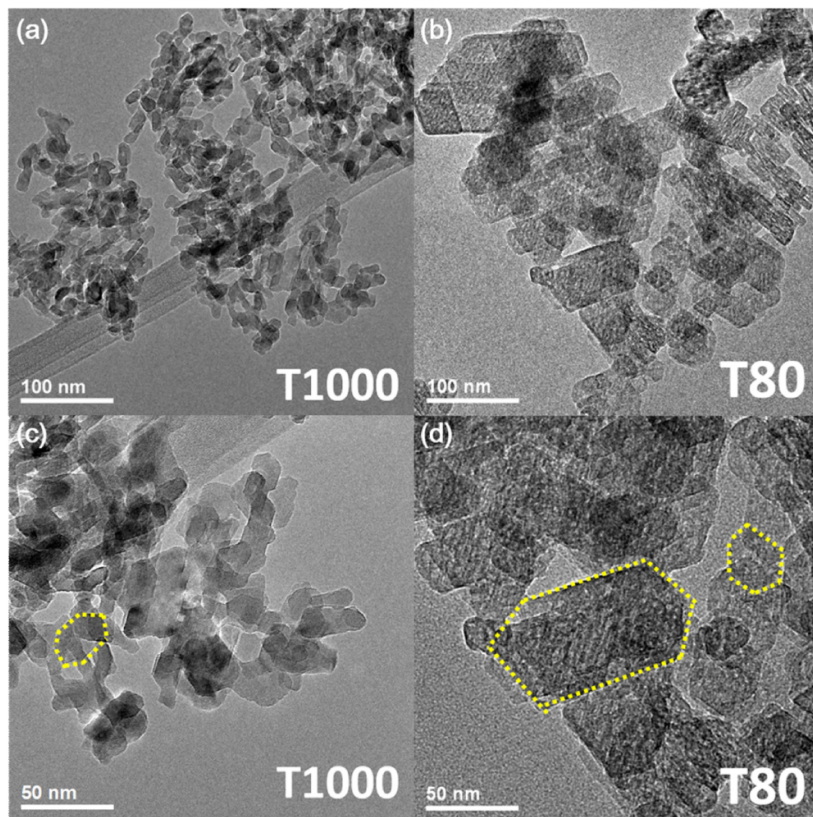


Fig. 11. TEM images for (a,c) T1000 and (b,d) T80.

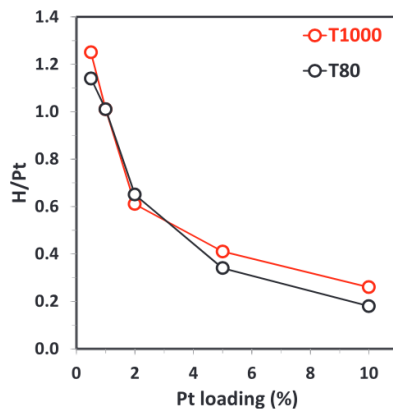


Fig. 12. H/Pt trend as a function of Pt loading for T1000 and T80 after calcination and reduction at 500 °C.

that of 1 wt% Pt/Al₂O₃. When we compare the Pt size distribution up to ~ 3 nm size shown in Fig. 7(c), (f) and (i), T80 exhibited a greater fraction of bigger Pt clusters than T150 and T110, which was consistent with the trend in H/Pt. However, these size differences are not straightforward when we consider the average Pt size change estimated based on H₂ chemisorption (3.5 nm for T150, 5.2 nm for T110 and 6.1 nm for T80), suggesting the intrinsic limitation of the local properties of TEM characterization. Fig. S4 showed the overall particle size distribution up to ~ 80 nm for 10 wt% Pt on T150, T110 and T80, but accurate quantification for large agglomerated Pt was difficult. In order to characterize the bigger Pt clusters, we carried out XRD analysis (Fig. 8). The figure showed diffraction peaks for Pt (111) at $2\theta = 39.8^\circ$, Pt (002) at $2\theta = 46.2^\circ$ and Pt (022) at $2\theta = 67.5^\circ$. Although the

diffraction peaks of Pt overlap with those of Al₂O₃, we can clearly observe the sharp peak of Pt(111), indicating that agglomerated Pt exists on 10 wt% Pt/Al₂O₃. Here, the Pt(111) peak intensities were the highest for 10 wt% Pt/T80, the intermediate for 10 wt% Pt/T110, and the lowest for 10 wt% Pt/T150, consistently showing that large agglomerated Pt clusters existed more on T80 than on T150 on Fig. S4(d). The estimation of Pt size using the Scherrer equation was not straightforward owing to the mixed Al₂O₃ peaks and the broad peaks of smaller Pt clusters. Despite a bimodal distribution for 10 wt% Pt/Al₂O₃, all the characterizations showed that T150 exhibit a higher Pt dispersion than T80 for both agglomerated Pt and small Pt clusters, clearly demonstrating that Pt can be more highly dispersed with increasing the number of sites of alumina.

Note here that utilizing multiple characterization techniques is important for understanding the heterogeneous nature of Pt/Al₂O₃. While TEM has limitations for Pt size measurements due to localized information, XRD reveals only larger Pt crystallites due to the low detectability for small Pt clusters (below ~ 2 nm) [44,45]. H₂ chemisorption shows the ensemble results for Pt dispersion, but a dominant contribution from smaller Pt clusters than agglomerated Pt because only small fractions of Pt are exposed for the agglomerated Pt clusters [45]. Using multiple characterization tools is critical for careful understanding Al₂O₃-supported Pt catalysts.

In summary, increasing the number of specific sites on alumina can increase Pt dispersion. However, the higher Pt dispersion does not arise from a gradual change in Pt cluster size, but from an increased fraction of highly dispersed Pt clusters (< 3 nm) on alumina under bimodal Pt size distribution involving large agglomerated Pt (> 10 nm) and small Pt clusters (< 3 nm).

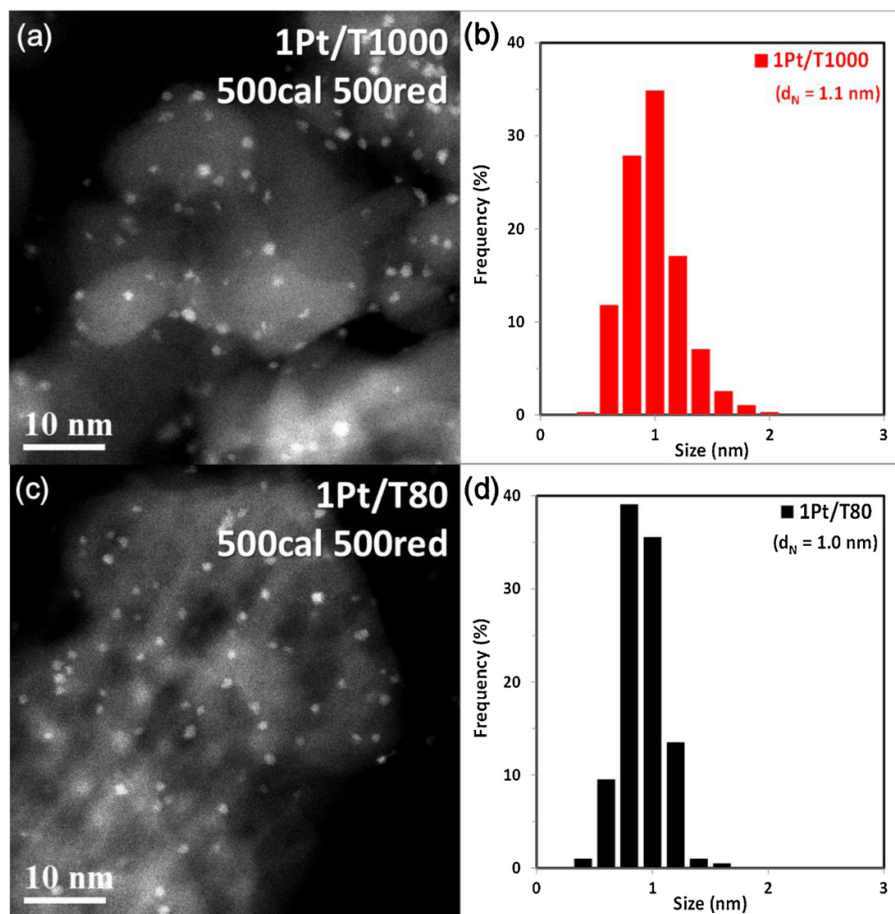


Fig. 13. STEM images and particle size distribution for (a,b) 1 Pt/T1000 and (c,d) 1 Pt/T80 after calcination and reduction at 500 °C.

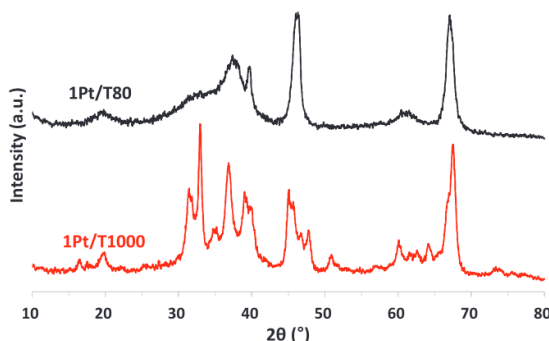


Fig. 14. XRD patterns for 1 Pt/T1000 and 1 Pt/T80 after calcination and reduction at 500 °C.

3.2. Properties of sites

In order to understand the effect of the properties of specific sites on Pt-Al₂O₃ interaction, we prepared two aluminas having similar number of sites with significantly different properties. We calcined T150 at 1000 °C for 3 h and labelled it as T1000, which was compared with T80.

Fig. 9 showed the ethanol TPD desorption profiles for T1000 and T80. The desorption temperature at the maximum rates (T_d) for T1000 was 34 °C higher than that of T80 (T150: 244.4 °C, and T80: 210 °C). This was consistent with previous reports that T_d shift into higher temperatures with increasing calcination temperature [19,24,33]. Note here that the amounts of dissociative ethanol desorbed were

practically the same for T1000 and T80 (1.8×10^{-4} mol/g for T1000 and 2.0×10^{-4} mol/g for T80).

The XRD pattern of T1000 (Fig. 10) showed two θ -Al₂O₃ peaks at $2\theta = 44.8^\circ$ and 47.8° that were clearly visible, apart from δ -Al₂O₃ peak at 45.8° , indicating that T1000 was phase-transformed into a mixture of δ -Al₂O₃ and θ -Al₂O₃ [46,47]. The T80 was previously confirmed as γ -Al₂O₃ (Fig. 1). The BET surface area of T1000 (Table 1) was $100 \text{ m}^2/\text{g}$, higher than that of T80 ($79 \text{ m}^2/\text{g}$). The N₂ adsorption/desorption profile for T1000 as shown in Fig. S2(b) was also similar with that of T80. The TEM images shown in Fig. 11 revealed that the morphology and particle size of T1000 were similar with those of precursor T150. The T1000 also had smaller particle size than T80 with the similar morphologies.

Fig. S5(a) showed the DRIFTS spectra for the surface hydroxyls of T1000 and T80 after activation at 380 °C. The spectrum of T1000 showed 3790 cm^{-1} bands that appeared with the decrease of the 3766 cm^{-1} peak compared to that of T80 (γ -Al₂O₃), and corresponded to the typical hydroxyl spectra for δ , θ -Al₂O₃, which was consistent with the δ , θ -Al₂O₃ bulk structure by XRD [34,38]. It should be noted that T1000 had a new type of surface hydroxyls at 3790 cm^{-1} , which is assigned as isolated hydroxyls on tetrahedral or octahedral Al species, although the exact assignments are still controversial [16,17,36,38–40].

Fig. S5(b) and Fig. S5(c) showed the DRIFTS spectra after pyridine adsorption at 100 °C on T1000 and T80. Fig. S5(c) showed that the relative ratio between the 1623 and 1614 cm^{-1} peak intensities for T1000 was lower than that of T80. Fig. S5(b) showed the perturbed surface hydroxyls during pyridine adsorption. Here, the 3790 cm^{-1}

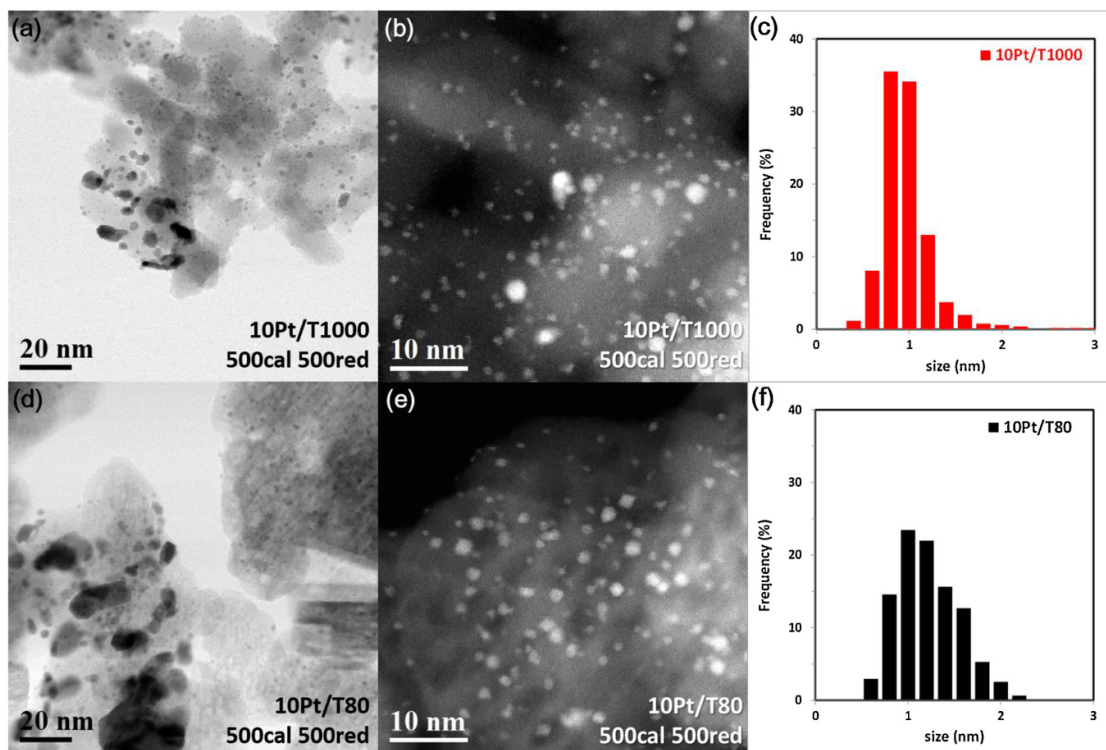


Fig. 15. Low magnification TEM, STEM images and particle size distribution below ~ 3 nm for (a–c) 10 Pt/T1000 and (d–f) 10 Pt/T80 after calcination and reduction at 500 °C.

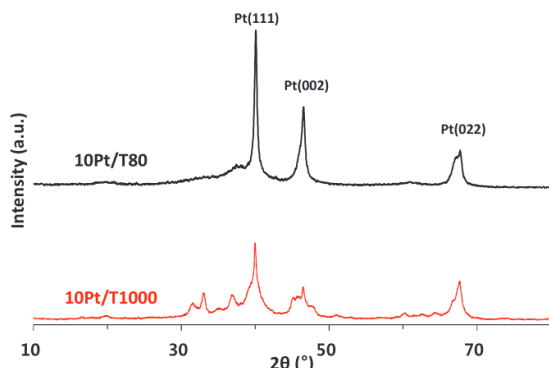


Fig. 16. XRD patterns for 10 Pt/T1000 and 10 Pt/T80 after calcination and reduction at 500 °C.

peaks were perturbed only in the case of T1000, also indicating a new type of surface hydroxyl was formed after the phase-transition to δ,θ -Al₂O₃. Overall, T1000 has the different acid site distribution compared to T80, which correlates with the higher T_d (34 °C) from ethanol TPD (different properties of sites).

In order to investigate the effect of the properties of sites for Pt-Al₂O₃ interaction, H₂ chemisorption was also carried out for Pt/T1000. Fig. 12 showed the H/Pt results obtained by H₂ chemisorption as a function of Pt loading from 0.5 to 10 wt%. Similar to the previous trend, H/Pt decreased with increasing Pt loading on T1000. At the loadings of 0.5–2 wt% Pt, H/Pt was practically the same on T1000 and T80. For 1 wt% Pt/Al₂O₃, H/Pt was 1.01 for T1000 and 1.01 for T80. However, interestingly, H/Pt was higher for T1000 than for T80 at higher Pt loading (5–10 wt%). At 10 wt% Pt/Al₂O₃, H/Pt was 0.26 for T1000 and 0.18 for T80, meaning that Pt was more well-dispersed on T1000 than on T80. Overall, the higher the T_d , the higher the Pt dispersion.

As previously discussed, T1000 and T80 have enough number of sites to disperse Pt at 0.5–1 wt% Pt. Therefore, the H/Pt value was close to 1, meaning almost all the Pt was exposed to the surface. However, with increasing Pt loading to 10 wt%, the two aluminas have insufficient sites to disperse all the Pt, leading to a decrease in H/Pt below 1. Here, note that T1000 had the same number of sites as T80 but higher T_d (by 34 °C), as revealed by ethanol TPD (Fig. 9). So, higher Pt dispersion on T1000 will be attributed to the properties of the sites on the alumina surface. A higher T_d on the alumina surface means that the Al³⁺ sites bind ethanol more strongly than those of T80, making it difficult to desorb as ethylene. Similarly, the alumina surface on T1000 anchors Pt more strongly than that of T80 does, and stabilizes Pt, leading to a higher dispersion on T1000 than on T80.

Considering the IR data (Fig. S5), T1000 exhibits a new type of isolated surface hydroxyl at 3790 cm⁻¹, which would contribute to a higher Pt dispersion on T1000. Consistently, some studies have reported that these isolated hydroxyls are likely to be related to Pt anchoring [48]. However, more detailed studies on the relationship between Pt and surface hydroxyls are still needed, which will be the future work.

The Pt dispersion was also confirmed by TEM measurements. Fig. 13 showed the representative STEM images for 1 wt% Pt/Al₂O₃ after calcination and reduction at 500 °C. The Pt clusters around ~ 1 nm was highly dispersed, consistent with the absence of diffraction peaks for Pt in XRD (Fig. 14). The Pt size distribution by measuring 400 clusters showed that the average particle diameter was 1.1 nm for T1000, and 1.0 nm for T80, indicating that the Pt sizes were similar between the aluminas, consistent with the same H/Pt by H₂ chemisorption.

Fig. 15 showed TEM and STEM images for 10 wt% Pt/Al₂O₃ after the same treatment with 1 wt% Pt/Al₂O₃. As the number of sites on T1000 is similar to that on T80, T1000 also showed a bimodal distribution, similar to the case of T80. When we compare the Pt size distribution up to ~ 3 nm size as shown in Fig. 15(c) and (f), T80

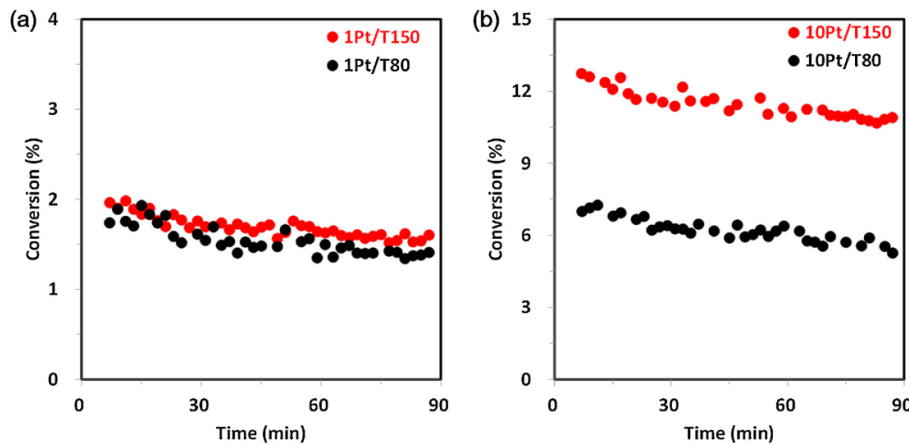


Fig. 17. Time-on-stream C₆H₆ hydrogenation profiles for (a) 1 Pt/T150 and 1 Pt/T80 and (b) 10 Pt/T150 and 10 Pt/T80.

Table 3

H/Pt value, benzene hydrogenation conversion and turnover frequencies for 1 Pt/T150, 1 Pt/T80, and 1 Pt/T1000 (top) and 10 Pt/T150, 10 Pt/T80, and 10 Pt/T1000 (bottom). Turnover frequencies were normalized based on H/Pt from hydrogen chemisorption.

Sample	H/Pt	Conversion (%)	TOF (C ₆ H ₆ /Pt · s)
1 Pt/T150	1.03	1.9	0.039
1 Pt/T80	1.01	1.9	0.039
1 Pt/T1000	1.01	2.0	0.042
10 Pt/T150	0.31	12.5	0.170
10 Pt/T80	0.18	7.1	0.166
10 Pt/T1000	0.26	9.6	0.156

showed more portion of bigger Pt clusters than T1000, which was consistent with the trend in H/Pt. However, these size differences are not significant when we consider the average Pt size change estimated by H₂ chemisorption (4.2 nm for T1000 and 6.1 nm for T80). Fig. S6 showed the overall particle size distribution up to ~80 nm for 10 wt% Pt/T80 and T1000, showing the bimodal distribution for 10 wt% Pt/T80 and T1000. However, accurate quantification for large agglomerated Pt was difficult. XRD analysis (Fig. 16) showed that the Pt(111) peak intensities were higher for 10 wt% Pt/T80 than 10 wt% Pt/T1000, indicating that more agglomerated Pt exists on T80 than on T1000. Again, the Pt size estimation was not accurate due to the overlapping of the alumina peak and underlying broadness of smaller Pt clusters. Despite the bimodal distribution for 10 wt% Pt/Al₂O₃, all the

characterizations showed that T1000 has a higher Pt dispersion than T80 for both agglomerated Pt and small Pt clusters, clearly demonstrating that Pt can be more highly dispersed with T_d increase on alumina surfaces.

3.3. Catalytic reaction: benzene hydrogenation

In order to study how the number and properties of sites affect the catalytic properties of Pt/Al₂O₃, we carried out C₆H₆ hydrogenation reaction. C₆H₆ hydrogenation has been one of the typical model reactions for supported metal characterization for decades [49–53]. We chose 1 wt% Pt/Al₂O₃ and 10 wt% Pt/Al₂O₃ for T150, T80, and T1000 model alumina after 500 °C calcination and reduction. C₆H₆ hydrogenation was carried out at 80 °C. Note that for each reaction, the same amount of catalyst was used: 6 mg for 1 wt% Pt/Al₂O₃ and 3 mg for 10 wt% Pt/Al₂O₃.

Fig. 17(a) showed the reaction profiles of C₆H₆ hydrogenation for 1 wt% Pt/T150 and 1 wt% Pt/T80. Catalyst deactivation was observed during the reaction, so the initial activity was estimated by linear extrapolation. Both 1 wt% Pt/T150 and 1 wt% Pt/T80 showed practically the same activity profile. The turnover frequency (TOF) normalized by H/Pt (Table 3) was 0.039 C₆H₆/Pt·s for 1 wt% Pt/T150 and 1 wt% Pt/T80. The TOF normalized by H/Pt (Table 3) was also practically the same, 0.170 and 0.166 C₆H₆/Pt·s for 10 wt% Pt/T150 and 10 wt% Pt/T80, respectively even though 10 wt% Pt/T150 showed much higher conversion than 10 wt% Pt/T80 as shown in Fig. 17(b). Previous characterization data showed that 1 wt% Pt/T150 and 1 wt% Pt/T80

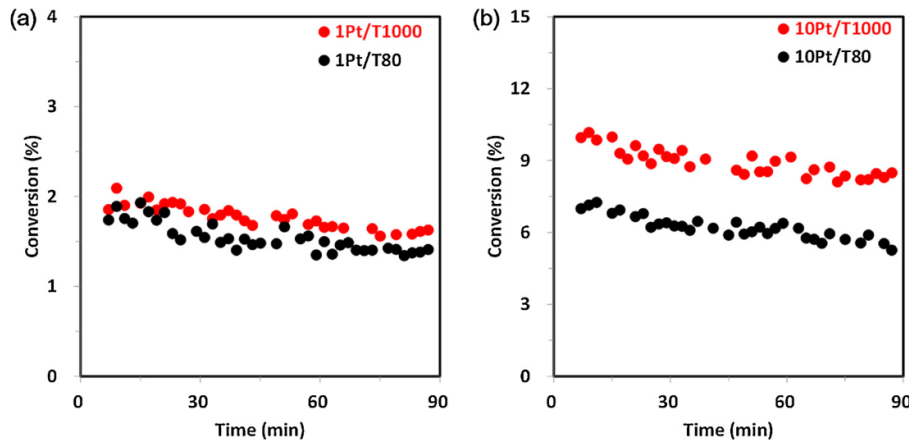


Fig. 18. Time-on-stream C₆H₆ hydrogenation profiles for (a) 1 Pt/T1000 and 1 Pt/T80 and (b) 10 Pt/T1000 and 10 Pt/T80.

had the same Pt dispersion, as confirmed by H₂ chemisorption and STEM. That's why the same reaction profile and TOF for 1 wt% Pt/T150 and 1 wt% Pt/T80. However, 10 wt% Pt/T150 (H/Pt=0.31) showed higher Pt dispersion than 10 wt% Pt/T80 (H/Pt = 0.18). In addition, the XRD and TEM results showed that agglomerated Pt and small Pt clusters coexist on 10 wt% Pt/Al₂O₃. Owing to a very low number of exposed sites on agglomerated Pt, the reaction is typically governed by the highly dispersed Pt clusters (< 3 nm). It suggests that the intrinsic activities of the Pt clusters (TOF) were the same, but the higher conversion for 10 wt% Pt/T150 than for 10 wt% Pt/T80 can be interpreted that more Pt clusters on 10 wt% Pt/T150 contributed the reaction, which contributed dominantly from highly dispersed Pt clusters.

Previous studies have reported that benzene hydrogenation is structure-insensitive, which means that the specific activity (TOF) is independent of Pt size [54,55]. However, other studies also reported that benzene hydrogenation is structure-sensitive [51,52]. Flores et al. reported that the structure sensitivity depended on pre-treatment of Pt/Al₂O₃ [52]. For high temperature reduction (450 °C), the specific activity increases with decreasing Pt dispersion up to H/Pt = 0.48 (structure-sensitive) and became constant at dispersion lower than H/Pt = 0.48 (structure-insensitive). However, at low reduction temperatures (100–300 °C), the reaction was structure-sensitive at the wide range of H/Pt values (0.04–0.88). Note that in this work our samples were reduced at 500 °C. The TOF at H/Pt = 1.0 was 0.039 C₆H₆/Pt·s, but increased to 0.166–0.17 C₆H₆/Pt·s at H/Pt = 0.18–0.31. Fig. S7 showed that the TOF value increased with decreasing H/Pt, but became constant at low Pt dispersions (H/Pt = 0.18–0.31), which is consistent with the results of Flores et al. However, detailed studies on whether benzene hydrogenation is structure-sensitive or not are beyond the scope of this work, because our conventional impregnated catalysts have broad size distribution of Pt clusters, and particularly bimodal distribution for 10 wt% Pt/Al₂O₃, which renders the determination of structure sensitivity difficult. The recent work by Somorjai group reported that benzene hydrogenation is moderately structure-sensitive for Pt nanoparticles carefully well-controlled in a narrow size distribution [51].

Subsequently, we studied the effect of the properties of the sites on alumina surfaces for benzene hydrogenation by comparing Pt/T1000 and Pt/T80. Fig. 18(a) showed the reaction profile for C₆H₆ hydrogenation for 1 wt% Pt/T1000 and 1 wt% Pt/T80. The initial conversion was 2.0% for 1 Pt/T1000 and 1.9% for 1 wt% Pt/T80, showing the similar activities. The TOF normalized by H/Pt (Table 3) was 0.042 C₆H₆/Pt·s for 1 wt% Pt/T1000 and 0.039 C₆H₆/Pt·s for 1 wt% Pt/T80. Similar to the earlier case of 1 wt% Pt/T150 and 1 wt% Pt/T80, 1 wt% Pt/T1000 showed Pt dispersion similar to that of 1 wt% Pt/T80, as evidenced from H/Pt and STEM. That's why 1 wt% Pt/T1000 showed the identical activity with 1 wt% Pt/T80. It is also reasonable to conclude that all the 1 wt% Pt/Al₂O₃ investigated for benzene hydrogenation (1 wt% Pt/T150, 1 wt% Pt/T80, and 1 wt% Pt/T1000) had similar Pt dispersions and intrinsic activities (TOF: 0.039–0.042 C₆H₆/Pt·s).

When we compare the TOF normalized by H/Pt (Table 3), the values were 0.156 C₆H₆/Pt·s for 10 wt% Pt/T1000 and 0.166 C₆H₆/Pt·s for 10 wt% Pt/T80, which were practically same. However, as shown in Fig. 18(b), 10 wt% Pt/T1000 showed higher conversion than 10 wt% Pt/T80. As previously discussed, the higher conversion for 10 wt% Pt/T1000 can be attributed to the higher number of Pt surface sites on 10 wt% Pt/T1000 than 10 wt% Pt/T80, which are dominated by the highly dispersed Pt clusters. When we compared this with 10 wt% Pt/T150 activity, 10 wt% Pt/T150 showed the higher conversion (12.5%) than 10 wt% Pt/T1000 (9.6%) because it has also more exposed Pt sites (H/Pt is 0.31 for 10 wt% Pt/T150, and 0.26 for 10 wt% Pt/T1000).

4. Conclusion

In this work, we investigated the effect of the number and properties

of specific sites on alumina surfaces on Pt-Al₂O₃ interaction by using XRD, ethanol TPD, DRIFTS, H₂ chemisorption, STEM and benzene hydrogenation as the model reaction. Here, we chose two sets of model aluminas having different number of sites with the identical properties (T150, T110 and T80) and different properties of sites with the same number (T1000, T80) based on ethanol TPD. Ethanol TPD showed that T150, T110, and T80 had similar T_d (208.5–210 °C) but different desorption amounts (3.8×10^{-4} mol/g for T150, 2.4×10^{-4} mol/g for T110, and 2.0×10^{-4} mol/g for T80). The T1000 showed higher T_d (by 34.4 °C) than T80 for the same number of sites (1.8×10^{-4} mol/g for T1000). The DRIFTS of surface hydroxyls showed that T150, T110, and T80 have similar type of surface hydroxyl groups, consistent with the similar T_d obtained from ethanol TPD. However, T1000 have a new type of surface hydroxyl at 3790 cm⁻¹, which is the origin of the different surface properties compared to T80.

After loading 0.5–10 wt% Pt onto these model aluminas, the Pt dispersion was analyzed by various characterization tools (H₂ chemisorption, XRD and STEM). At low Pt loadings (0.5–1 wt% Pt), the number of sites was sufficient to disperse all the Pt, leading to highly dispersed Pt clusters without any aggregated Pt. Therefore, all the model aluminas showed highly dispersed Pt, as evidenced by similar H/Pt values (~1.0) from H₂ chemisorption. However, at higher loading (10 wt% Pt), the number of Pt were higher than that of anchoring sites, resulting in aggregated Pt evidenced by the sharp Pt(111) peak in XRD, along with small Pt clusters (below ~3 nm), revealed by STEM. Under bimodal particle size distribution, both T150 and T1000 exhibited higher Pt dispersion, with greater portion of smaller Pt clusters and less aggregated Pt, leading to different catalytic properties (higher conversion) for benzene hydrogenation compared to T80. All the results clearly demonstrate that Pt can be more dispersed with increasing number of sites and interaction strength. This fundamental understanding provides an important perspective for designing Al₂O₃-based supported catalysts.

Acknowledgements

We acknowledge the financial support from the National Research Foundation (NRF) (No. 2016R1A5A1009405, 2017R1A2B4007310) and the Ministry of Trade, Industry & Energy (10050509, N0001754). We also thanks HEESUNG CATALYSTS CORP for their financial supports.

Appendix A. Supplementary data

Supplementary material related to this article can be found, in the online version, at doi:<https://doi.org/10.1016/j.apcata.2018.10.004>.

References

- [1] T.V. Choudhary, S. Banerjee, V.R. Choudhary, Appl. Catal. A: Gen. 234 (2002) 1.
- [2] P. Gelin, M. Primet, Appl. Catal. B: Environ. 39 (2002) 1.
- [3] M.R. Rahimpour, M. Jafari, D. Iranshahi, Appl. Energy 109 (2013) 79.
- [4] J.J.H.B. Sattler, J. Ruiz-Martinez, E. Santillan-Jimenez, B.M. Weckhuysen, Chem. Rev. 114 (2014) 10613.
- [5] I.E. Beck, V.I. Bukhtiyarov, I.Y. Pakharukov, V.I. Zaikovsky, V.V. Kriventsov, V.N. Parmon, J. Catal. 268 (2009) 60.
- [6] C.H. Hu, C. Chizallet, C. Mager-Maury, M. Corral-Valero, P. Sautet, H. Toulhoat, P. Raybaud, J. Catal. 274 (2010) 99.
- [7] M. Vaarkamp, J.T. Miller, F.S. Modica, D.C. Koningsberger, J. Catal. 163 (1996) 294.
- [8] H. Matsushashi, S. Nishiyama, H. Miura, K. Eguchi, K. Hasegawa, Y. Iizuka, A. Igarashi, N. Katada, J. Kobayashi, T. Kubota, T. Mori, K. Nakai, N. Okazaki, M. Sugioka, T. Umeki, Y. Yazawa, D. Lu, Appl. Catal. A: Gen. 272 (2004) 329.
- [9] Y. Yazawa, N. Takagi, H. Yoshida, S.-i. Komai, A. Satsuma, T. Tanaka, S. Yoshida, T. Hattori, Appl. Catal. A: Gen. 233 (2002) 103.
- [10] R.M. Mironenko, O.B. Belskaya, V.P. Talsi, T.I. Gulyaeva, M.O. Kazakov, A.I. Nizovskii, A.V. Kalinkin, V.I. Bukhtiyarov, A.V. Lavrenov, V.A. Likhobolov, Appl. Catal. A: Gen. 469 (2014) 472.
- [11] J.E. Park, B.B. Kim, E.D. Park, Korean J. Chem. Eng. 32 (2015) 2212.
- [12] A. Gorczyca, V. Moizan, C. Chizallet, O. Proux, W.D. Net, E. Lahera, J.L. Hazemann, P. Raybaud, Y. Joly, Angew. Chem. Int. Ed. 126 (2014) 12634.
- [13] I.H. Cho, S.B. Park, S.J. Cho, R. Ryoo, J. Catal. 173 (1998) 295.

J. Lee et al.

Applied Catalysis A, General 569 (2019) 8–19

- [14] J.H. Kwak, J. Hu, D. Mei, C.-W. Yi, D.H. Kim, C.H.F. Peden, L.F. Allard, J. Szanyi, *Science* 325 (2009) 1670.
- [15] M. Digne, P. Sautet, P. Raybaud, P. Euzen, H. Toulhoat, *J. Catal.* 211 (2002) 1.
- [16] M. Digne, P. Sautet, P. Raybaud, P. Euzen, H. Toulhoat, *J. Catal.* 226 (2004) 54.
- [17] G. Busca, *Catal. Today* 226 (2014) 2.
- [18] M. Trueba, S.P. Trasatti, *Eur. J. Inorg. Chem.* (2005) (2005) 3393.
- [19] J. Lee, H. Jeon, D.G. Oh, J. Szanyi, J.H. Kwak, *Appl. Catal. A: Gen.* 500 (2015) 58.
- [20] W. Cai, S. Zhang, J. Lv, J. Chen, J. Yang, Y. Wang, X. Guo, L. Peng, W. Ding, Y. Chen, Y. Lei, Z. Chen, W. Yang, Z. Xie, *ACS Catal.* 7 (2017) 4083.
- [21] C. Barra, L. Plais, K. Larmier, E. Devers, M. Digne, A.-F. Lamic-Humblot, G.D. Pirngruber, X. Carrier, *J. Am. Chem. Soc.* 137 (2015) 15915.
- [22] J. Lee, E.J. Jang, H.Y. Jeong, J.H. Kwak, *Appl. Catal. A: Gen.* 556 (2018) 121.
- [23] D. Shi, H. Wang, L. Kovarik, F. Gao, C. Wan, J.Z. Hu, Y. Wang, *J. Catal.* 363 (2018) 1.
- [24] J. Lee, E.J. Jang, J.H. Kwak, *J. Catal.* 345 (2017) 135.
- [25] C. Mager-Maury, C. Chizallet, P. Sautet, P. Raybaud, *ACS Catal.* 2 (2012) 1346.
- [26] M. Paulis, H. Peyrard, M. Montes, *J. Catal.* 199 (2001) 30.
- [27] J.H. Kwak, D. Mei, C.H.F. Peden, R. Rousseau, J. Szanyi, *Catal. Lett.* 141 (2011) 649.
- [28] J.H. Kwak, J. Lee, J. Szanyi, C.H.F. Peden, *Catal. Today* 265 (2016) 240.
- [29] C. Morterra, G. Magnacca, *Catal. Today* 27 (1996) 497.
- [30] J.L. Lemaitre, P.G. Menon, F. Delannay, F. Delannay (Ed.), Characterization of Heterogeneous Catalysts, Marcel Dekker, New York, 1984, pp. 299–365.
- [31] R.J. Madon, M. Boudart, *Ind. Eng. Chem. Fundam.* 21 (1982) 438.
- [32] K.S.W. Sing, D.H. Everett, R.A.W. Haul, L. Moscou, R.A. Pierotti, J. Rouquerol, T. Siemieniewska, *Pure Appl. Chem.* 57 (1985) 603.
- [33] J.Z. Hu, S. Xu, J.H. Kwak, M.Y. Hu, C. Wan, Z. Zhao, J. Szanyi, X. Bao, X. Han, Y. Wang, C.H.F. Peden, *J. Catal.* 336 (2016) 85.
- [34] T.K. Phung, A. Lagazzo, M.Á. Rivero Crespo, V. Sánchez Escribano, G. Busca, *J. Catal.* 311 (2014) 102.
- [35] T.K. Phung, C. Herrera, M.Á. Larribia, M. García-Díéguez, E. Finocchio, L.J. Alemany, G. Busca, *Appl. Catal. A: Gen.* 483 (2014) 41.
- [36] G. Busca, V. Lorenzelli, G. Ramis, R.J. Willey, *Langmuir* 9 (1993) 1492.
- [37] J.B. Peri, *J. Phys. Chem.* 69 (1965) 220.
- [38] G. Busca, V. Lorenzelli, V.S. Escribano, R. Guidetti, *J. Catal.* 131 (1991) 167.
- [39] H. Knözinger, P. Ratnasamy, *Catal. Rev.-Sci. Eng.* 17 (1978) 31.
- [40] A.A. Tsyanenko, P.P. Mardilovich, *Faraday Trans.* 92 (1996) 4843.
- [41] T.K. Phung, L.P. Hernández, A. Lagazzo, G. Busca, *Appl. Catal. A: Gen.* 493 (2015) 77.
- [42] K. Larmier, C. Chizallet, N. Cadran, S. Maury, J. Abboud, A.-F. Lamic-Humblot, E. Marceau, H. Lauron-Pernot, *ACS Catal.* 5 (2015) 4423.
- [43] H.C. Yao, M. Sieg, H.K. Plummer, *J. Catal.* 59 (1979) 365.
- [44] S.J.L. Billinge, I. Levin, *Science* 316 (2007) 561.
- [45] L. Spenadel, M. Boudart, *J. Phys. Chem.* 64 (1960) 204.
- [46] L. Kovarik, M. Bowden, D. Shi, N.M. Washton, A. Andersen, J.Z. Hu, J. Lee, J. Szanyi, J.H. Kwak, C.H.F. Peden, *Chem. Mater.* 27 (2015) 7042.
- [47] M. Nguefack, A.F. Popa, S. Rossignol, C. Kappenstein, *Phys. Chem. Chem. Phys.* 5 (2003) 4279.
- [48] I. Malpartida, M.A.L. Vargas, L.J. Alemany, E. Finocchio, G. Busca, *Appl. Catal. B: Environ.* 80 (2008) 214.
- [49] S.D. Lin, M.A. Vannice, *J. Catal.* 143 (1993) 539.
- [50] S.D. Lin, M.A. Vannice, *J. Catal.* 143 (1993) 563.
- [51] V.V. Pushkarev, K. An, S. Alayoglu, S.K. Beaumont, G.A. Somorjai, *J. Catal.* 292 (2012) 64.
- [52] A.F. Flores, R.L. Burwell, J.B. Butt, *J. Chem. Soc. Faraday Trans.* 88 (1992) 1191.
- [53] K.M. Bratlie, H. Lee, K. Komvopoulos, P. Yang, G.A. Somorjai, *Nano Lett.* 7 (2007) 3097.
- [54] J. Barbier, A. Morales, P. Marecot, R. Maurel, *Bull. Soc. Chim. Belg.* 88 (1979) 569.
- [55] M. Koussathana, D. Vamvouka, H. Economou, X. Verykios, *Appl. Catal.* 77 (1991) 283.

